LA-UR-94-481 revised March 6, 1995

Modeling Flows with Curved Detonation Waves

RALPH MENIKOFF and KLAUS S. LACKNER

Theoretical Division, Los Alamos National Laboratory, Los Alamos, NM 87545

and

BRUCE G. BUKIET

Department of Mathematics, Center for Applied Mathematics and Statistics

New Jersey Institute of Technology, Newark, NJ 07102

ABSTRACT

The non-zero width of a curved detonation front has a significant effect on its propagation. Physically, the curvature effect is a small but important correction. In numerical simulations, the curvature effect tends to be greatly exaggerated due to an artificially large width of an underresolved wave. In the context of reactive fluid flow, a detonation wave consists of a lead shock followed by a thin reaction zone. The curvature effect is determined by the dynamics within the reaction zone; in particular, the competition between a source term for the rate of chemical energy release and a geometric source term due to front curvature. When the width of the reaction zone is small compared to the radius of curvature of the front, the reaction zone can be approximated as quasi-steady and be modeled locally by a system of ordinary differential equations (ODEs) in which the front curvature enters as a parameter. Front curvature breaks the Galilean invariance and the quasi-steady approximation is only valid in a distinguished frame determined by both the front curvature and the tangential velocity gradients ahead of the front. The quasi-steady ODEs determine the reaction zone profile to leading order and can be viewed as an extension of the ZND model. However, the source terms in the ODEs lead to modified Hugoniot jump conditions that take into account front curvature and reaction zone width. When the reaction zone is underresolved, a calculation in effect reduces to a "capturing algorithm" in which the burn model plays an analogous role for detonation waves as artificial viscosity does for shock waves. In particular, the reaction zone has an unphysically large width that is proportional to the cell size. As a consequence of the modified jump conditions, the numerical reaction zone width gives rise to an artificial curvature effect. This causes numerical solutions to depend on cell size and the orientation of a detonation front relative to the grid. Two algorithms that eliminate numerical curvature effects are discussed; detonation shock dynamics and front tracking.

NOMENCLATURE

A	cross sectional area of stream tube
C_V	specific heat at constant volume
D	detonation speed, underdriven or overdriven
$D(\kappa_f)$	underdriven detonation speed for diverging wave with front curvature κ_f
$D_{\Delta x}(R)$	numerical detonation speed for a rate stick of radius R and cell size Δx
E	specific internal energy
P	pressure
Q	specific heat released in chemical reaction
R	radius of rate stick or principle radii of curvature of detonation front
S	specific entropy
T	temperature
V	specific volume
c	frozen sound speed
k	rate constant for Arrhenius rate law
m	mass flux through detonation front
t	time coordinate
u	particle velocity
u_{ahead}	particle velocity ahead of front in distinguished frame of reference
w	reaction zone width
x	spatial coordinate along stream tube

Greek Symbols

δ	reaction order for Arrhenius rate law
γ	adiabatic exponent
κ	divergence of stream lines
κ_f	geometric front curvature
λ	mass fraction of reaction products
ρ	material density
σ	thermicity
$\Delta[f]$	jump in quantity f across the detonation wave
Δx	cell size of computational mesh

Script Symbols

$\mathcal{E}$	total specific energy
$\mathcal{R}$	specific reaction rate

Other Symbols

∇_T	gradient in tangent plane to the front
$\langle f \rangle$	average value of f in reaction zone
$\overline{f}$	arithmetic average of f at front and back of reaction zone

subscripts

0	state ahead of detonation front
1	state behind reaction zone
CJ	Chapman-Jouguet state for planar detonation

1. Introduction

The reactive Euler equations provide the framework for a description of fluid flows in an explosive material. With one irreversible exothermic reaction, a large class of reaction rate laws leads to the Zel'dovich–von Neumann–Doering (ZND) model [1] in which a detonation wave consists of a lead shock followed by a thin reaction zone. The ZND model predicts that the state behind a planar steady detonation wave is on the strong branch of the detonation shock Hugoniot and is independent of the reaction zone profile. Moreover, the detonation wave with the minimum detonation speed, Chapman-Jouguet (CJ) detonation, has a sonic state behind the detonation front and corresponds to an underdriven detonation.

In contrast to the planar case, the reaction zone dynamics can not be neglected for curved detonation waves. A well known and important example is the diameter effect; the dependence in a rate stick of the steady-state detonation speed on the diameter of the explosive charge [2–5]. The detonation speed in a rate stick is less than the minimum planar CJ detonation speed, and therefore it is clear that the ZND model must be modified for a curved detonation wave.

In general, the local front curvature affects the propagation of both underdriven and overdriven detonation waves. We call this the curvature effect. The diameter effect is a special case for a steady-state underdriven diverging detonation wave propagating in a cylindrical tube. We show that the curvature effect results from the interaction between a geometric source term due to the curvature of the detonation front and a source term for the rate at which energy is released by the chemical reaction. Because the curvature effect depends on the reaction zone dynamics, it can not be determined solely from the Hugoniot jump conditions and the equation of state of the reaction products.

When the reaction zone width is small compared to the radius of curvature of the detonation front, we show in section 3 that the reaction zone can be modeled locally by a system of ODEs that describe one-dimensional quasi-steady waves. These ODEs determine the reaction zone profile to leading order and can be viewed as an extension of the ZND model that accounts for the curvature of the detonation front. The geometric source term due to front curvature breaks the Galilean invariance of the ODEs. Consequently, the quasi-steady approximation is only valid in the distinguished frame in which the cross sectional area of a local stream tube is to leading order time independent. The distinguished frame is uniquely determined by the front curvature and the tangential velocity gradient ahead of the detonation front. It is not the local shock-attached frame. Furthermore, in the distinguished frame the geometric source term, which represents the local divergence of the stream lines, is determined by the mean curvature of the detonation front.

The quasi-steady ODEs have been used previously for diverging waves to determine the underdriven detonation wave speed as a function of mean front curvature, $D(\kappa_f)$ [6–9]. The function $D(\kappa_f)$ characterizes enough of the reaction zone dynamics to describe the diameter effect. It is used in the Detonation Shock Dynamics (DSD) model to propagate an underdriven diverging detonation wave using a Huygen's construction in which the local wave speed depends on the front curvature [10–12].

Our derivation of the quasi-steady ODEs shows that the model is also the leading order approximation for overdriven detonation waves in both diverging and converging geometry [13]. For a curved front, the detonation speed and the state behind the detonation wave depend on the reaction zone dynamics as well as the equation of state of the detonation products. The qualitative properties of the detonation wave curve, which is the curvature dependent analog of the ZND detonation Hugoniot, are described in section 4. In particular, it is shown that an underdriven diverging detonation wave does not correspond to a weak detonation wave on a partially burnt detonation Hugoniot.

The curvature dependent detonation wave curves differ from the standard planar detonation Hugoniot. Consequently, the standard Hugoniot jump conditions, which express the conservation laws across a wave, must be modified to account for the non-zero reaction zone width and the front curvature. The modified Hugoniot jump conditions are derived in section 5. The leading order correction terms to the jump conditions are proportional to the product of the front curvature, the reaction zone width and terms involving two averaged quantities within the reaction zone. A considerable simplification over our previous version of the modified jump conditions [14] is obtained by consistently working only to leading order. The correction terms are not Galilean invariant and must be evaluated in the distinguished reference frame we identified in section 3. Moreover, we show that the qualitative properties of the detonation wave curve described in section 4 can be easily deduced from the modified jump conditions.

The length and time scales of the reaction zone are much smaller than those of the bulk flow. Consequently, it is computationally expensive and frequently impractical to resolve the reaction zone. When the reaction zone is not resolved, a calculation in effect reduces to a "capturing algorithm" in which the burn model plays an analogous role for detonation waves as artificial viscosity does for shock waves. The reaction zone will have a greatly exaggerated width that is proportional to the cell size. The modified jump conditions we derived apply to the solutions of both the partial differential equations (PDEs) and numerical algorithms written in conservation form. An important consequence of the modified jump conditions is that the numerical reaction zone width results in an artificial curvature effect which is mesh dependent. A numerical example illustrating this effect is discussed in section 2. A systematic numerical study of the diameter effect varying the cell size was carried out by Donguy & Legrand [15]. Their results show that with a typical cell size used for calculations the numerical curvature effect can be significantly larger than the real physical curvature effect. As the cell size is decreased and the reaction zone is better resolved, the artificial numerical curvature effect decreases. However, along with higher resolution 2-D flow within the reaction zone may become important and modify the curvature effect.

Section 6 discusses two-dimensional effects that the quasi-steady one-dimensional model neglects. Highly resolved 2-D calculations show that the reaction zone is subject to transverse instabilities [16–18]. The numerical results indicate that the amplitude of the transverse instabilities saturate and a long wavelength average of the detonation front is well behaved. Because of the simplified burn models, these calculations of the reaction zone instability are only expected to be qualitative in nature. Considering (i) that there is insufficient data to determine the physical rates in detail, (ii) that the chaotic structure of the reaction zone is very sensitive to the assumed reaction rates, and (iii) that the heterogeneities in solid explosives are neglected in the models, the detailed short wavelength structure of the reaction zone predicted by the calculations can not possibly be quantitatively accurate for real explosives. Thus, the most one could expect from high resolution calculations of the reaction zone is the statistics of the short wavelength fluctuations caused by the transverse instabilities. Without a very fine mesh, the transverse wave structure can not be numerically resolved. Consequently, a coarse mesh excludes the transverse instabilities. Hence short wavelengths are damped out by numerical truncation errors and an underresolved calculation is tantamount to a long wavelength approximation. Numerical calculations on moderately fine meshes, which in the reaction zone partly resolve the longitudinal flow but not the transverse flow, are an approximation to the quasi-steady one-dimensional model we have analyzed.

Thus, one is led to a computational dilemma for the choice of mesh resolution: (i) with a coarse mesh the reaction zone is not resolved and the curvature effect is mesh dependent; (ii) with a moderately fine mesh the reaction zone is partially resolved and the numerical algorithm smoothes the physics in an uncontrolled manner; (iii) with a very fine mesh fine detail of the reaction zone is expensive to calculate and quantitatively inaccurate for any real explosive. Since the fine detail affects the propagation of the detonation front, a mesh dependent calibration of an effective rate law would be required to reproduce the experimental wave propagation data.

At minimum, to avoid a mesh dependent curvature effect, a fine mesh is needed for the reaction zone. Computational efficiency would require an adaptive mesh. Since the fine mesh would track the detonation front, an adaptive mesh would in effect be a form of tracking algorithm. Moreover, fine meshes require small time steps and are computationally expensive. In section 7, two alternative tracking algorithms are discussed; detonation shock dynamics and front tracking. These algorithms, in effect, incorporate the analytical structure of the quasi-steady one-dimensional reaction zone model. They can be calibrated to propagate accurately a detonation wave in accordance with empirical bulk wave propagation data (long wavelength approximation) without resolving the reaction zone.

DSD is simpler but only appropriate for an underdriven diverging detonation wave propagating into a medium with a constant state [10, 11]. On the other hand front tracking is a general algorithm applicable to both underdriven and overdriven detonation waves. It incorporates the effect on the propagation of a detonation wave from acoustic waves overtaking the front from behind and from a non-uniform state ahead of the front [19–21].

2. Diameter Effect and Mesh Dependence

The mesh dependence of the wave speed on a propagating detonation wave is illustrated in the computational results of Donguy & Legrand [15] for the diameter effect of a TATB based explosive. They calculated an underdriven detonation wave in an unconfined cylindrical rate stick using a 2-D Eulerian reactive hydro code and the Forest Fire burn model. In the Forest Fire model [22, 23] the reaction rate is a function of pressure which is fit to wedge test data for the distance of run to detonation (Pop plot) [24].

In their calculations, Donguy & Legrand systematically varied the diameter of the rate stick and the cell size. The calculated wave speed was compared to experiment. Their main conclusion was that a minimum of 4 to 6 cells in the reaction zone is needed for an accurate simulation. However, their results can also be interpreted as an example of the mesh dependent numerical curvature effect that we will be analyzing. We start by reviewing their numerical results.

A measure of the magnitude of the curvature effect is the dimensionless velocity deficit

$$\Delta\widetilde{D} = \frac{D_{\mathrm{CJ}} - D_{\Delta x}(R)}{D_{\mathrm{CJ}}} \tag{2.1}$$

where $D_{\Delta x}(R)$ is the numerical detonation speed for a rate stick of radius R computed with cell size Δx, and $D_{\mathrm{CJ}} = D_0(\infty)$ is the planar detonation speed. Using the data in Table I of Ref. 15, the mesh dependence of the curvature effect, *i.e.*, the velocity deficit as the cell size is varied, is plotted in Fig. 1. The figure shows that the numerical curvature effect exceeds the experimental curvature effect. Furthermore, the numerical curvature effect increases with cell size. Though the experimental curvature effect is only a few percent, for a moderate mesh size >> 1 mm, the numerical curvature effect can be much larger (over ten percent), and can cause significant errors in wave propagation. The small cell size needed for an accurate simulation implies that a uniform mesh would not be feasible for many applications.

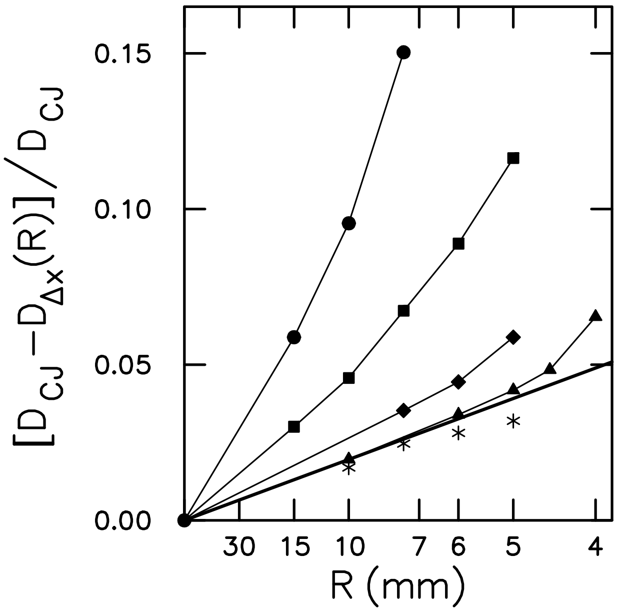

Fig. 1: Mesh dependence of curvature effect; numerical data from Table I of Ref. 15. Thick solid line is fit to experimental data. Circle, square, diamond and triangle are calculations with cell size of $\Delta x = 0.5$, 0.25, 0.125 and 0.075 mm respectively. The value of $D_{\rm CJ}$ from the experiment (7.666 mm/μs) and the numerical simulation (7.650 mm/μs) differ slightly. The symbol $*$ corresponds to the extrapolation of the last two points to $\Delta x = 0$ assuming second order convergence.

For a fixed rate stick diameter, Fig. 2 shows the convergence rate of the detonation speed as the cell size is varied. The slope on a log-log scale indicates that the convergence is second order. Furthermore, for a 12 mm diameter rate stick as $\Delta x \rightarrow 0$ the detonation wave speed appears to converge to $\Delta\widetilde{D}_0 = 0.028$. This is 15% smaller than the experimental value of 0.033. The numerical error in the curvature effect is slightly larger than the error in the experimental data; Ref. 15, Fig. 2.

Figure 3 shows the reaction zone width as the cell size is varied. The number of cells in the reaction zone increases as the resolution is increased but the reaction zone length decreases with cell size. This observation is the key to understanding the numerical curvature effect. In the subsequent sections, we explain the physical curvature effect in terms of a modification to the Hugoniot jump condition due to reaction zone width and front curvature. The same analysis, which is based on the conservation laws, applies to any numerical algorithm written in conservation form. This explains how the numerical width of the front leads to a numerical curvature effect which dominates the real physical effect.

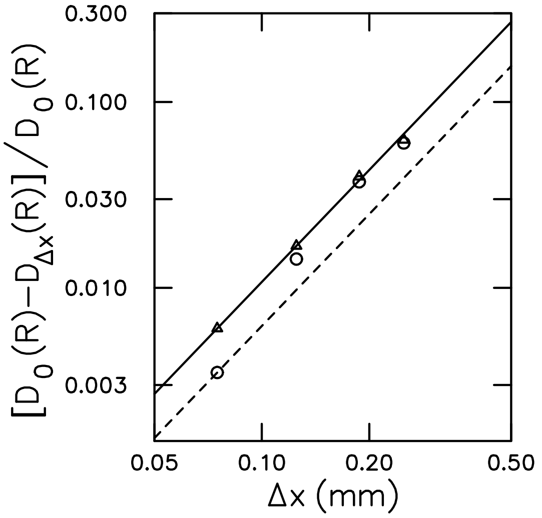

Fig. 2: Convergence rate of detonation speed for 12 mm diameter rate stick; numerical data from Table I of Ref. 15. Dashed line and circles are based on the experimental value for $D_0(6\,\mathrm{mm})$ and solid line and triangles on the extrapolation from the last two points. The curves are plotted on a log-log scale. The slope of the straight line fits correspond to second order convergence.

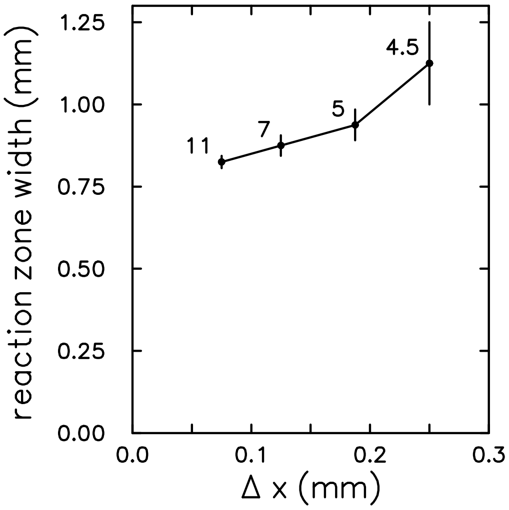

Fig. 3: Numerical width of reaction zone for 12 mm diameter rate stick; numerical data from Table I of Ref. 15. Error bars correspond to cell width. The number of cells in the reaction zone is next to each data point.

3. Reaction Zone Model

In this section, we develop a local analysis for the reaction zone of a curved detonation wave starting from the PDEs for reactive fluid flow. The analysis is based on two approximations; in a distinguished frame the flow in the reaction zone is one-dimensional normal to the detonation front and quasi-steady. Although this analysis is developed in the context of a generalization of the ZND model from a planar to a curved detonation wave, the essential ideas apply to any curved wave of non-zero width. The detailed analysis applies to a detonation front away from boundaries and away from wave patterns formed by the interaction of detonation waves. In these other cases, tangential flow within the reaction zone is significant and causes the one-dimensional approximation to break down [25].

As in the ZND model we neglect transport phenomena; *i.e.*, viscosity and heat conduction. In this model a detonation wave consists of a discontinuous shock wave followed by a thin reaction zone. We consider the lead shock to be the detonation front.

3.1 One-Dimensional Approximation

A curved detonation wave is assumed to have the following properties:

(1) The front is smooth.

(2) The wave speed normal to the front is slowly varying with front position.

(3) The reaction zone width w is much smaller than the principal radii of curvature of the front.

(4) The wave speed changes by a small amount in the transit time for a particle through the reaction zone.

These assumptions correspond to a long wavelength, low frequency approximation in which transverse flows and transverse instabilities are neglected or averaged over. Tacit assumptions of this nature are also essential for nearly all numerical simulations of practical applications involving detonation waves.

It follows from these assumptions that derivatives of the fluid variables tangent to the front are much smaller than those normal to the front. Therefore, within the reaction zone the dominant variation of the variables is in the normal direction and thus the flow in the reaction zone can locally be approximated as one-dimensional. Since the front is curved, normals to the front are not parallel. Two dimensional effects from the geometry can be accounted for by source terms in a one-dimensional model.

Consider a small areal patch on the detonation front. The streak lines through this patch form a flow tube. Let A be the cross sectional area of the flow tube. The variation of the cross sectional area accounts for the dominant two-dimensional effect on the flow. Locally, the reaction zone is described by the 1-D equations for reactive flow in a duct of variable cross sectional area

$$(\rho A)_t + (\rho A u)_x = 0 \,, \tag{3.1}$$

$$(\rho A u)_t + \left(\rho A \left[u^2 + PV\right]\right)_x = PA_x \,, \tag{3.2}$$

$$(\rho A \mathcal{E})_t + (\rho A u \left[\mathcal{E} + PV\right])_x = -PA_t \,, \tag{3.3}$$

$$(\rho A \lambda)_t + (\rho A u \lambda)_x = \rho A \mathcal{R} \,, \tag{3.4}$$

where ρ, u, E and λ are the fluid density, particle velocity along the stream line, specific internal energy (thermal + chemical) and mass fraction of the reaction products ($\lambda = 0$ unburnt, $\lambda = 1$ completely burnt), $V = 1/\rho$ is the specific volume, $\mathcal{E} = \frac{1}{2}u^2 + E$ is the total specific energy, $P(V, E, \lambda)$ is the pressure, and $\mathcal{R}(V, E, \lambda)$ is the specific reaction rate.

It is important to note that in the 1-D approximation only the area and not the shape of the flow tube enters into the equations. The flow tube is not Galilean invariant. There are two special frames for which to leading order $\partial_t A = 0$: (i) the co-moving frame, *i.e.*, the frame moving with the local front velocity and (ii) the normal frame, *i.e.*, the frame for which the flow is normal to the front across the local patch. In these frames, the only geometric term that enters into Eqs. 3.1–3.4 is the local divergence of the streak lines

$$\kappa = \lim_{A \to 0} (\partial_x A / A) \ . \tag{3.5}$$

The co-moving frame is not a good choice because $\kappa(x)$ is not *a priori* known. The frame in which the flow is on average normal to the front is unique. For this distinguished frame, we show that κ is the front curvature and to leading order is independent of x.

Let the normal to the front be directed from the reacted fluid towards the unreacted fluid. The geometric front curvature is

$$\kappa_f = 1/R_1 + 1/R_2 = 2 \times (\text{mean curvature}) \tag{3.6}$$

where R_i are the two principal (signed) radii of curvature. With our choice of normal, $\kappa_f > 0$ for a diverging wave and $\kappa_f < 0$ for a converging wave. The planar case corresponds to zero curvature. κ_f is also zero if the principal curvatures are equal in magnitude but have opposite signs.

We start by considering a 1-D detonation front in a 2-D flow. Suppose $\vec{r}_0$ is a point on the front. Let x and y be the coordinates normal and tangential to the front at $\vec{r}_0$. We can choose our origin such that $\vec{r}_0 = (0, 0)$. As shown in Fig. 4, we can find a Galilean transformation to a frame such that the flow is normal to the front in a neighborhood of $\vec{r}_0$. This requires that the velocity at $\vec{r}_0$ be $(u_{\text{ahead}}, 0)$ where $\kappa_f u_{\text{ahead}} = \partial_y u_y$. Because the

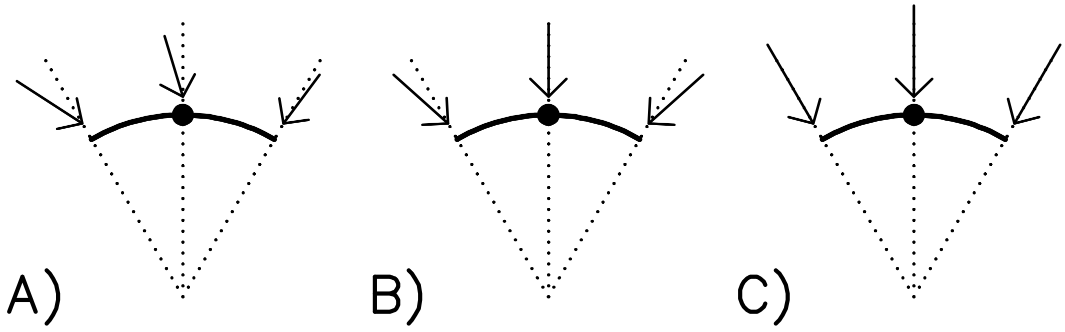

Fig. 4: A) An arbitrary velocity field in the neighborhood of point $\vec{r}_0$ on a curved front. $\vec{r}_0$ is shown as a solid dot and the front as thick line. Dotted lines are normal to the front. B) The first transformation removes the tangential component of the velocity field at point $\vec{r}_0$. To first order the field is now antisymmetric around the normal through $\vec{r}_0$. C) The second transformation adjusts the normal velocity at $\vec{r}_0$ so that the tangential velocity components vanish in neighborhood of $\vec{r}_0$.

tangential velocity components are constant to leading order, the flow within the reaction zone remains normal to the front. Thus, in this Galilean frame, the local flow through $\vec{r}_0$ can be described using the geometrical coordinates defined by the instantaneous front and its normals. In this distinguished frame, $\partial_t A = 0$ and the streak lines coincide with the normal coordinate lines. Furthermore,

$$\partial_x A/A = \pm\kappa_f \left[1 + O(\kappa_f w')\right] , \tag{3.7}$$

where the + and − signs are for right facing and left facing waves respectively, and w' is the distance a particle travels in traversing the reaction zone.

For convenience, from here on we choose the orientation of our coordinate system to correspond to a right facing detonation wave; the normal to the front is in the $+\hat{x}$ direction and hence mass enters the reaction zone from the right, *i.e.*, $D - u > 0$. We note that the reaction zone width

$$w = \int_0^1 \frac{d\lambda}{\mathcal{R}} (D - u) \tag{3.8}$$

and the distance a particle travels in traversing the reaction zone

$$w' = \int_0^1 \frac{d\lambda}{\mathcal{R}}\, u \tag{3.9}$$

are comparable provided $u_{\text{ahead}} < D$.

Next we consider a 2-D front in a 3-D flow. Let x be the normal direction and y and z correspond to the directions of the principle radii of curvature. We can choose the origin to correspond to the point $\vec{r}_0$ and $\hat{x}$ to the normal direction at $\vec{r}_0$. The previous strategy of transforming to a frame in which the flow is normal to the front would require that

$$\frac{u_{\text{ahead}}}{R_y} = \partial_y u_y \quad \text{and} \quad \frac{u_{\text{ahead}}}{R_z} = \partial_z u_z \ . \tag{3.10}$$

These relations can only be satisfied if the derivatives of the velocity satisfy the relation $R_z/R_y = \partial_y u_y / \partial_z u_z$. Thus, in general it is not possible to choose a Galilean frame such that the streamlines follow a normal to the front. However, we show that there is a frame in which the cross sectional area of the stream tube coincides with that of the tube formed by the normals.

Consider the velocities $\vec{u}_N$ normal to the front and $\vec{u}_T$ tangential to the front. In a neighborhood of $\vec{r}_0$, the normal is given to leading order by $\hat{n} = (1,\, y/R_y,\, z/R_z)$. In the local coordinate system, the velocity has the form $\vec{u} = (u_{\text{ahead}}, u_y, u_z)$ with $u_y(0) = 0$ and $u_z(0) = 0$. To leading order, it follows that

$$\begin{aligned}
\hat{n}\cdot\vec{u} &= u_{\text{ahead}} \\
\vec{u}_T &= \vec{u} - (\hat{n}\cdot\vec{u})\hat{n} \\
&= (0,\ u_y - y\, u_{\text{ahead}}/R_y,\ u_z - z\, u_{\text{ahead}}/R_z) \\
\nabla_T\cdot\vec{u}_T &= \nabla_T\cdot\vec{u} - \kappa_f\, u_{\text{ahead}}
\end{aligned}$$

where $\nabla_T = \hat{y}\partial_y + \hat{z}\partial_z$ is the gradient in the tangent plane. We choose the frame in which

$$\kappa_f\, u_{\text{ahead}} = \nabla_T\cdot\vec{u}(\vec{r}_0) \ . \tag{3.11}$$

In this frame $\nabla_T\cdot\vec{u}_T = 0$. The transformation is possible except in the case of zero mean curvature with a non-zero tangential velocity divergence.

A divergence free flow in two dimensions preserves area. Hence, $\vec{u}_T$ does not affect the area of the flow tube and may be neglected. Even though the streak lines are neither normal to the front nor do they lead to a stationary flow tube, in the distinguished frame which is on average normal, the cross sectional area of the flow tube is everywhere the same as for the geometric coordinate frame spanned by the front and its local normal. In order that w' is comparable to w, we require $|\nabla_T \cdot \vec{u}| \ll |\kappa_f D|$. Then, to leading order $\partial_t A = 0$ and $\kappa = \kappa_f\,[1 + O(\kappa_f w)]$, where we use the notation $O(\kappa_f\, w)$ in place of the cumbersome expression $O(w/|R_y| + w/|R_z|)$. As an aside, we note that to leading order the hour glass or bow tie mesh instability in Lagrangian algorithms is also related to the fact that the flow in a stream tube is not affected by area preserving shape changes.

To summarize, there is a distinguished frame in which the flow is on average normal to the front. In this frame, the 1-D approximation is valid when $|\kappa_f w| \ll 1$, and the geometric source terms from the divergence of the streamlines are related to the front curvature when $|\nabla_T \cdot \vec{u}| \ll |\kappa_f D|$. After solving for the reaction zone profile in the distinguished frame, a Galilean transformation can be used to determine the reaction zone profile in any other frame. In particular, by adding a constant to the velocity, the profile can be transformed to match the velocity at the front ahead of the detonation wave. This procedure is necessary for tracking algorithms in order for them to be well defined.

3.2 Quasi-Steady Approximation

The time and length scales in the reaction zone are much smaller than those for the bulk flow. In the small transit time for a particle to travel through the reaction zone, the dynamics of the reaction zone hardly varies. In particular, the front curvature and wave speed are nearly constant. Consequently, we can assume that the reaction zone profile varies adiabatically, *i.e.*, rapidly equilibrates to slow changes in the bulk flow. This is the equivalent for PDEs to neglecting the high frequencies in a stiff system of ODEs.

To first order in $\kappa_f w$, asymptotic analysis shows that ∂_t can be replaced by $-D\partial_x$ where D is the detonation wave speed [6, 7, 25, 26]. As a consequence, the PDEs can be reduced to a system of ODEs for the quasi-steady reaction zone profile. After some algebraic manipulation, the ODEs can be cast in the following form

$$[\rho(D-u)]_x = \rho u \kappa_f \ , \tag{3.12}$$

$$\left[\rho(D-u)^2 + P\right]_x = \rho(D-u)u\kappa_f \ , \tag{3.13}$$

$$\left[E + PV + \tfrac{1}{2}(D-u)^2\right]_x = 0 \ . \tag{3.14}$$

$$(u-D)\lambda_x = \mathcal{R} \tag{3.15}$$

where x is the distance relative to the front. For these equations, κ_f and D are to be treated as parameters.

The reaction zone profile is determined by an initial value problem. The boundary conditions are the state behind the lead shock with wave speed D and the velocity ahead of the shock given by 3.11, and a completely burnt state ($\lambda = 1$) at the end of the reaction zone. The allowed values of the wave speed D are discussed in section 4. It is important to note that the source terms are not Galilean invariant and hence the ODEs are only valid in the "normal frame." In particular, these ODEs do not apply in the co-moving (or shock-attached) frame.

In general, the detonation wave curve depends on two parameters; κ_f and $\nabla_T \cdot \vec{u}_{\text{ahead}}$. For a solid explosive the ambient state typically has a constant velocity. Consequently, $\nabla_T \cdot \vec{u}_{\text{ahead}} = 0$ and the wave curve only depends on one parameter, κ_f. The DSD algorithm tacitly makes this assumption. Certainly, for gaseous explosives both parameters may be important; *e.g.*, the oblique detonation wave engine proposed for hypersonic propulsion.

We note that the PDEs Eqs. 3.1–3.4 and the related ODEs Eqs. 3.12–3.15 have been used previously to describe quasi 1-D reactive flow in a nozzle [27–29]. For the purpose of describing the curvature effect, we are applying these equations to a local flow tube and are assuming that $\kappa_f w$ is small.

Eqs. 3.12–3.15 represent a generalization of the ZND model to a curved detonation wave. In the limit of either planar geometry or zero reaction zone width they reduce to the standard ZND model. The equations apply locally with the front curvature and wave speed entering as parameters. Their quasi-steady solution is accurate to $O\big((\kappa_f w)^2\big)$. As a consequence of the source terms, the right hand side of Eqs. 3.12 and 3.15, the ODEs do not have first integrals. Hence the detonation wave curve depends on the dynamics of the reaction zone as well as on the equation of state. This can be interpreted as a competition between a source term for the rate of energy released by the chemical reaction and a geometric source term representing the divergence of the streamlines due to front curvature.

In section 5, modified Hugoniot jump conditions are derived from Eqs. 3.12–3.14 by applying the conservation laws to a wave with a non-zero width. The reasoning is quite general. A curved shock wave would have a similar curvature effect as we are describing for a detonation wave. Usually, the curvature effect of a shock wave is very small and can be neglected. However, if a relaxation process (such as ionization, dissociation, or radiation) or numerical dissipation leads to a large shock width then a shock wave would also exhibit a significant curvature effect. A detonation wave has two properties that make the curvature effect stand out: (1) The standard jump conditions predict a minimum detonation velocity. Measuring a detonation velocity below the minimum, as occurs in a rate stick experiment, can not be explained by moving along the Hugoniot curve. (2) The energy released by an underdriven detonation wave causes the flow behind the wave to be supersonic relative to the front. Hence, complications from a rear boundary condition are avoided.

4. Curvature Effect

The locus of end states of the reaction zone is called the detonation wave curve. It plays a similar role in analyzing the wave structure of solutions to the reactive flow equation as the shock Hugoniot does for non-reactive fluid flow. The detonation wave curve is determined by the ODEs for the quasi-steady reaction zone profile, Eqs. 3.12–3.15. Because the detonation wave curve accounts for the curvature effect and depends on two local parameters κ_f and $\nabla_T \cdot \vec{u}$, it differs from the usual detonation shock Hugoniot that describes planar detonation waves.

The quasi-steady ODEs apply to both diverging and converging detonation waves. The sign of the source term $\kappa_f u$ has an important effect on the detonation wave curve [13]. In particular, an underdriven detonation is usually associated with a diverging wave. However, the initial velocity which is determined by the transverse velocity divergence ahead of the wave also affects the geometric source term. With a sufficiently large convergent flow ahead of the detonation wave, a diverging front can behave like a convergent wave. To understand this behavior we discuss the critical points of the ODEs in the presence of the addition degree of freedom from the velocity gradient ahead of the detonation front.

This section highlights the departures from the conventional ZND model in the context of a simple constitutive relation and rate law. We show that the standard properties of the Hugoniot locus and Rayleigh line must be modified to accommodate the presence of curvature and reaction zone width. Even for small $\kappa_f w$ the effect on the detonation wave curve can be significant. In the next section, we show that the qualitative dependence of the detonation wave curve on the curvature is quite general and does not depend on the specifics of the simple model discussed here.

4.1 Structure of ODEs

Eqs. 3.12–3.15 can be put in the form

$$-[c^2-(D-u)^2]\,\frac{d}{dx}\begin{pmatrix} V \\ D-u \\ \lambda \end{pmatrix} = \begin{pmatrix} [c^2\sigma\mathcal{R}-(D-u)^2u\kappa_f]\times V/(D-u) \\ (\sigma\mathcal{R}-u\kappa_f)\times c^2 \\ [c^2-(D-u)^2]\times\mathcal{R}/(D-u) \end{pmatrix} \tag{4.1}$$

where $c^2 = \partial_\rho P|_{S,\lambda}$ is the square of the frozen sound speed, $\sigma = (\rho c^2)^{-1}\,\partial_\lambda P|_{V,E}$ is the thermicity, and the Bernoulli function $E+PV+\frac{1}{2}\,(D-u)^2$ is a constant of the motion. The Bernoulli function is also constant across the lead shock and hence its value is determined by the state ahead of the detonation wave.

Let $x=0$ be the detonation front. For fixed D and κ_f the reaction zone profile is determined by the initial value problem with $\lambda(0)=0$, and $V(0)$ and $u(0)$ the values behind a shock with wave speed D and ahead velocity given by Eq. 3.11. It follows from the properties of a shock wave that the flow at the start of the reaction zone is subsonic relative to the front, $|D-u(0)|<c(0)$. Typically, for an explosive, $\sigma\mathcal{R}$ is initially much larger than $u\kappa_f$. Thus, for a right facing wave each component on the right hand side of Eq. 4.1 is initially positive and hence V, $D-u$ and λ initially are increasing functions as x decreases behind the front.

It is important to note that when the quasi-steady approximation is valid, the relative velocity $D-u$ does not vanish. From the equation for the mass flux Eq. 3.12, it follows that $\rho(D-u)$ is approximately constant and hence $D-u$ can not change sign. As a result, the right hand side of Eq. 4.1 is not singular.

The allowed values for the detonation wave speed are affected by the critical points of the ODEs; *i.e.*, the points for which all source terms or the right hand side of Eq. 4.1 vanish. It follows from Eq. 4.1 that a critical point occurs only when both

$$c^2 - (D-u)^2 = 0 \tag{4.2}$$

$$\sigma\mathcal{R} - u\kappa_f = 0 \tag{4.3}$$

are satisfied.

The critical points depend on D and κ_f. For an irreversible exothermic reaction, $\sigma > 0$ and $\mathcal{R} \geq 0$. In the standard case ($u_{\text{ahead}} = 0$ and hence $u > 0$), it follows from Eq. 4.3 that a critical point in the physical domain $0 < \lambda < 1$ can occur only in diverging geometry, $\kappa_f > 0$. Planar geometry, $\kappa_f = 0$, is a degenerate case and the critical point can occur at the end of the reaction zone $\lambda = 1$ when $\mathcal{R}$ vanishes. In general, $\nabla_T \cdot \vec{u}$ affects D and u. When $\nabla_T \cdot \vec{u}$ is sufficiently large, u will change sign and a critical point can occur in converging geometry ($\kappa_f < 0$).

The critical point is the only allowable sonic point that can occur within the reaction zone. A reaction profile through the critical point is transonic. The flow behind the critical point is supersonic. Since an acoustic wave can not overtake a sonic point, the region of the reaction zone between the critical point and the detonation front decouples from the flow behind the detonation wave. This case corresponds to an underdriven detonation wave in which the reaction is self-sustaining. Such an underdriven detonation wave has the minimum allowable wave speed. The decoupling of an underdriven detonation is the key property on which the DSD algorithm is based. Eqs. 4.1 have been used to determine the underdriven wave speed $D(\kappa_f)$ for a general reaction rate and a general equation of state [9].

The entire reaction zone is subsonic for all other profiles that do not go through a critical point and terminate at $\lambda = 1$. These have wave speeds $D > D(\kappa_f)$ and correspond to overdriven detonation waves. The flow behind the reaction zone can influence an overdriven detonation wave. Overdriven waves are essential for describing cylindrically or spherically converging detonations [30, 31]. They also have been studied experimentally [32, 33]. Even steady state overdriven converging detonation waves have been observed; see [26], chpt. XI, sec. 2.2. The detonation wave curve characterizes the propagation of the overdriven detonation waves. In section 7.2 we discuss how this information may be used in a numerical simulation.

For $D < D(\kappa_f)$, the trajectories of the ODEs terminate on the sonic locus (see *e.g.*, Ref. 13) and do not correspond to valid quasi-steady reaction zone profiles. The state of an underdriven planar detonation wave (CJ state) can be determined geometrically in the P–V plane as the point on the detonation shock Hugoniot tangent to the Rayleigh line. The CJ detonation speed is then determined by the slope of the Rayleigh line. For a curved detonation wave, the minimum detonation speed is determined by the reaction zone dynamics. It depends on the equation of state, the reaction rate and the two parameters κ_f and u_{ahead}.

4.2 Detonation Wave Curve

In this section, we discuss the qualitative effect that front curvature has on the detonation wave curve. To simplify the analysis, an explicit equation of state and rate law are used.

We assume an ideal gas equation of state

$$PV = (\gamma - 1)[E - (1-\lambda)Q] \ , \tag{4.4}$$

$$C_V T = E - (1-\lambda)Q \ , \tag{4.5}$$

where T is temperature. The adiabatic exponent γ, the specific heat release Q and the specific heat C_V are constants. The frozen sound speed and thermicity are

$$c^2 = \gamma PV = \gamma(\gamma-1)C_V T \ , \tag{4.6}$$

$$\sigma = (\gamma - 1)Q/c^2 \ . \tag{4.7}$$

For this example, the entropy

$$S = S_0 + C_V \log(PV^\gamma / P_0 V_0^\gamma) \tag{4.8}$$

is independent of λ corresponding to a reaction for which the number of molecules does not change.

We further assume an Arrhenius rate law

$$\mathcal{R} = k\,(1-\lambda)^\delta \exp(-T_a/T) \tag{4.9}$$

where k is the rate constant, δ is the reaction order, and T_a is the activation temperature.

Combining Eq. 4.6 with the constancy of the Bernoulli function we have

$$c^2 = \gamma(\gamma-1)C_V T = c_0^2 + (\gamma-1)\left[\tfrac{1}{2}\,(D-u_0)^2 - \tfrac{1}{2}\,(D-u)^2 + \lambda Q\right] \ . \tag{4.10}$$

As a consequence, c and T and hence $\mathcal{R}$ are functions u and λ only. Therefore, the u and λ components of Eq. 4.1 decouple from the V component. Since κ_f and D are constants, the dynamics of u and λ is determined by an autonomous pair of ODEs, which are equivalent to

$$\frac{d(D-u)}{d\lambda} = \frac{c^2\,(\sigma\mathcal{R} - u\kappa_f)\cdot(D-u)}{[c^2-(D-u)^2]\,\mathcal{R}} \ , \tag{4.11}$$

and the standard phase plane analysis applies [7, 13, 27, 34, 35]. When $\kappa_f = 0$, $\mathcal{R}$ drops out of Eq. 4.11. Hence for the planar detonation wave profile, as a function of λ, the velocity and the thermodynamic variables are independent of the reaction rate. In addition, for a planar profile $D-u$ is monotonic.

As an example, we use the same parameters as in Ref. 13: for the equation of state $\gamma = 1.2$, $Q = 50$ and $C_V = 5$; for the rate law $k = 3$, $\delta = 0.5$ and $T_a = 10$ and for the ambient unreacted state $P_0 = 1$, $u_0 = 0$ and $\rho_0 = 1$. For this case the planar detonation waves are stable in one dimension [36, 37]. For the CJ detonation wave $D_{\rm CJ} = 6.81$, $P_{\rm CJ} = 21.53$, $V_{\rm CJ} = 0.557$, $u_{\rm CJ} = 3.02$ and $w_{\rm CJ} = 4.11$.

The detonation wave curve for a given κ_f is obtained by varying D and integrating the ODEs for the reaction zone profile. For our illustrative explosive, Fig. 5 shows the locus in the P–V plane of end states of the reaction zone profiles. The planar case corresponds to the standard detonation shock Hugoniot which is determined entirely from the equation of state and the Hugoniot jump conditions. The minimum detonation speed in the planar case is the CJ detonation speed. The diverging and converging cases are shown for $\kappa_f = \pm 0.02$. As a consequence of the non-zero reaction zone width, neither a converging nor diverging detonation wave satisfy the standard jump conditions. As seen in Fig. 6, the minimum detonation wave speed decreases with increasing front curvature.

There is a qualitative difference between the detonation locus for the converging and diverging case. The diverging detonation locus has an isolated point in the P–V plane that corresponds to a supersonic state relative to the front. It has the minimum detonation wave speed and is the analog of the CJ state for a planar underdriven detonation wave. This special point is determined from an 'eigenvalue' like problem for the trajectory through the critical point (separatrix) [7, 9, 35, 38, 39]. The eigenvalue, $D(\kappa_f)$, plays a key role in detonation shock dynamics [10–12]. Near the isolated underdriven detonation state, the wave curve has a structure similar to that of a phase transition; *i.e.*, split waves and composite waves [13]. The transition from the underdriven state to the overdriven branch of the wave curve is accomplished by complicated transients due to the sonic point in the underdriven wave profile [25]. These transients are beyond the scope of this paper.

Even though the underdriven detonation wave corresponds to an isolated point in the P–V plane, the wave speed is continuous along the detonation wave curve. Moreover, the detonation wave speed of a curved front is not determined by the slope of the Rayleigh line. This can be seen in Figs. 5 and 6 where the state corresponding to an underdriven diverging detonation wave lies above the Rayleigh line through the planar CJ state but has a lower detonation wave speed. We also note in Fig. 5 that the underdriven diverging detonation state lies slightly below the weak branch of the planar detonation Hugoniot. Thus, the state behind an underdriven diverging detonation wave can not be derived from the standard Hugoniot jump conditions.

In converging geometry the locus of final states is a single connected curve. For the minimum detonation wave speed, at the end of the reaction zone the profile has an infinite

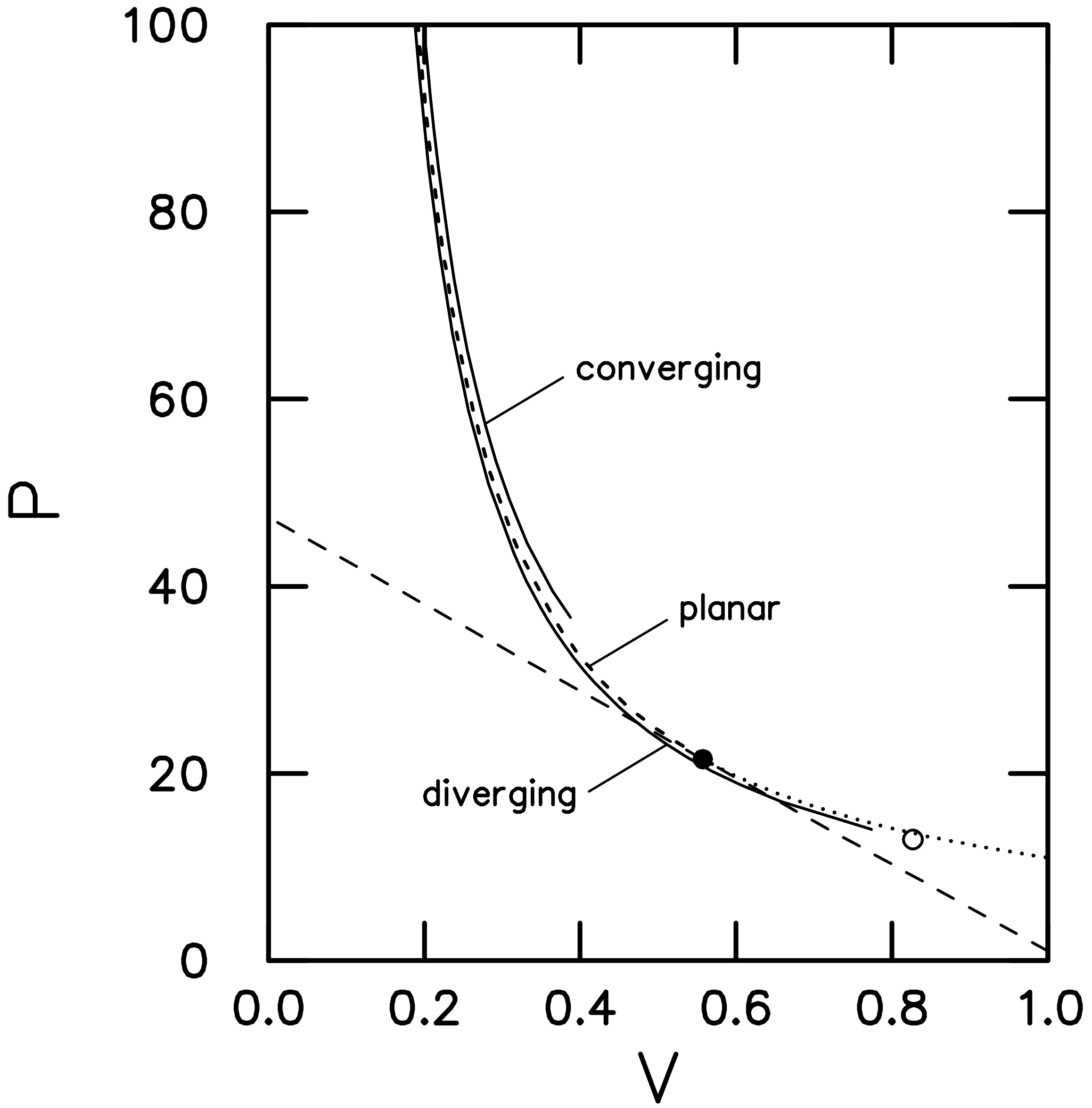

Fig. 5: The locus in the P–V plane of detonation wave final states. Diverging and converging geometry are represented by the solid lines for $\kappa_f = \pm 0.02$. The short-dashed and dotted lines are the strong and weak branch of the planar Hugoniot. The Rayleigh line through the planar CJ state is shown as a long-dashed line. The planar CJ state is shown with a solid circle and the underdriven diverging wave with an open circle. The initial state is $P = 1$ and $V = 1$.

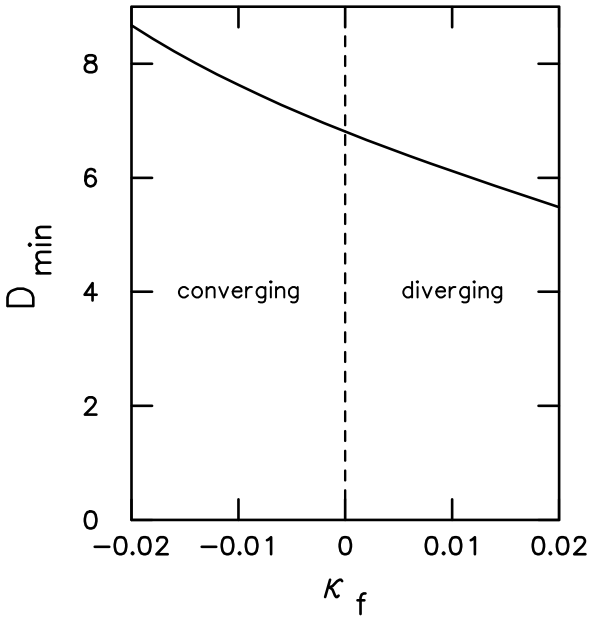

Fig. 6: The minimum detonation wave speed versus curvature. Both the converging and diverging cases are shown.

derivative [13]. Such a singularity suggests that in the neighborhood of a sonic point the model is not quite adequate. Physically, the singularity is regularized either by transport effects (such as viscosity or heat conduction) or by time dependence in the reaction zone, *i.e.*, the quasi-steady assumption breaks down [25]. In practice, convergent flow leads to an overdriven detonation wave and the exact nature of the singularity is not important.

The sonic point at the end of the reaction zone for the planar CJ detonation is also exceptional. From Eqs. 3.15 and 4.9, a finite reaction zone requires the reaction order be $\delta < 1$. As $\lambda \to 1$ for a CJ detonation, it follows from Eqs. 4.10 and 4.11 that $c^2 - (D_{\rm CJ} - u)^2 \sim (1-\lambda)^{\frac{1}{2}}$. Hence,

$$\frac{d}{dx}(D_{\rm CJ} - u) \sim \mathcal{R}\frac{d}{d\lambda}(D_{\rm CJ} - u) \sim (1-\lambda)^{\delta - \frac{1}{2}} \ . \tag{4.12}$$

For a finite derivative, $\delta \geq \frac{1}{2}$. Viscosity involves the second derivative which is

$$\frac{d^2}{dx^2}(D_{\rm CJ} - u) \sim (\delta - \tfrac{1}{2}) \cdot (1-\lambda)^{2\delta - \frac{3}{2}} \ . \tag{4.13}$$

Therefore, to neglect viscosity at the end of a CJ detonation requires either $\delta = {}^1/_2$ or $\delta \geq {}^3/_4$. This detailed dependence of the detonation profile near the sonic point on the reaction order is due to the simplicity of the burn model (single burn variable λ and neglect of transport effects) and should not be taken too seriously. We show in section 5 that the behavior of a detonation wave is dominated by a few integral quantities related to the conservation laws and is affected little by the peculiarities of this model. By adjusting a few parameters many different models can be made to fit the integral quantities and thus can reasonably reproduce the available experimental data. Consequently, model parameters need not be physically meaningful in order to fit the data.

For an underdriven diverging detonation wave, in the self-sustaining region of the reaction zone between the detonation front and the sonic point, only part of the available chemical energy is released; *i.e.*, at the sonic point $\lambda < 1$. For an ideal explosive, the CJ detonation wave speed is given in the strong shock limit $Q \gg c_a^2$ by $D_{\mathrm{CJ}}^2 = 2(\gamma^2 - 1)Q$. This raises the question as to whether the underdriven detonation wave speed decreases with curvature due to the lower energy available to drive the wave. The locus of CJ states on the partially burnt detonation shock Hugoniot (as λ is varied) and the locus of the sonic point from solving the ODEs (as κ_f is varied) are shown in Fig. 7. It is clear that the reaction zone dynamics is not adequately described by the value of λ at the sonic point. Rather the interplay between energy release and curvature determines an underdriven detonation.

To show the effect of curvature and initial velocity divergence, for a fixed detonation wave speed relative to the ambient state, the loci of the end states of the reaction zone in the P–V plane are plotted in Fig. 8. The solid line shows the variation with front curvature for the usual case of the ambient state ahead of the detonation at rest. As the curvature increases the pressure increases. Moreover, the curved detonation lies between the planar Rayleigh line and the planar Hugoniot curve. This is consistent with Fig. 5 which shows the curvature lowering the wave curve. We show in the next section that these qualitative features are independent of the equation of state and the reaction rate.

Also shown in Fig. 8 by dots is the variation of the end state with the velocity divergence for fixed κ_f. The dots nearly lie on the solid line. Thus the two parameters κ_f and $\nabla_T \cdot \vec{u}$ appear to trace out a single curve. Since E and $D - u$ are determined from P and V by the equation of state and the Bernoulli equation, it follows that the entire

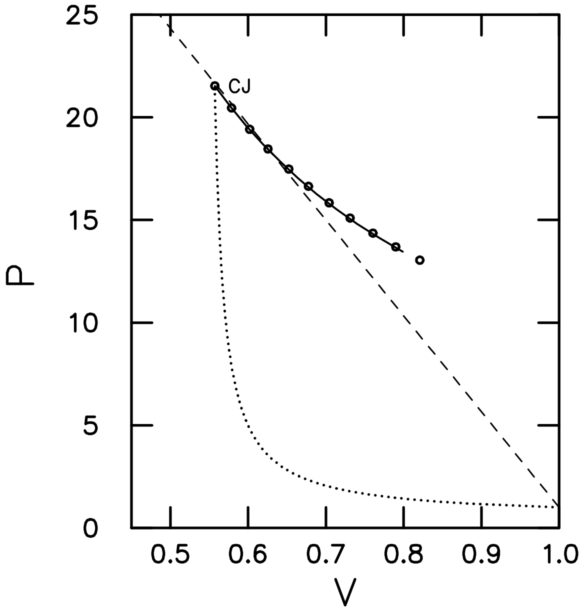

Fig. 7: Comparison of the loci of underdriven diverging detonation waves and partially burnt planar detonation waves. Diverging waves are parametrized by the front curvature and planar waves by the burn fraction. The dotted line is the locus of partially burnt sonic points. The dashed line is the Rayleigh line through the planar CJ state. The solid line is the locus of sonic points of diverging detonations. The circles define the locus of states at the end of the reaction zone.

end state corresponds. Hence for fixed D, front curvature and velocity divergence have a qualitatively similar effect.

It is a surprising result that κ_f and u_{ahead} have the same effect since there is no apparent symmetry in the ODEs for the quasi-steady reaction profile Eq. 4.1. The near coincidence of the loci can be partially understood by analyzing the entropy change across the detonation wave.

We conjecture that the entropy profile $S(\lambda)$ behind the lead shock is nearly independent of κ_f and u_{ahead} and only depends strongly on the mass flux through the detonation front. We have verified this numerically for a number of cases. For large values of Q, this conjecture is plausible but a rigorous proof is lacking. This entropy constraint would explain that in Fig. 8 the curved detonation state lies very close to the isentrope through the planar detonation state. Hence, the two parameter family of end states has been reduced to a single curve. However, as the wave speed is varied, the pairs (κ_f, u_{ahead}) that

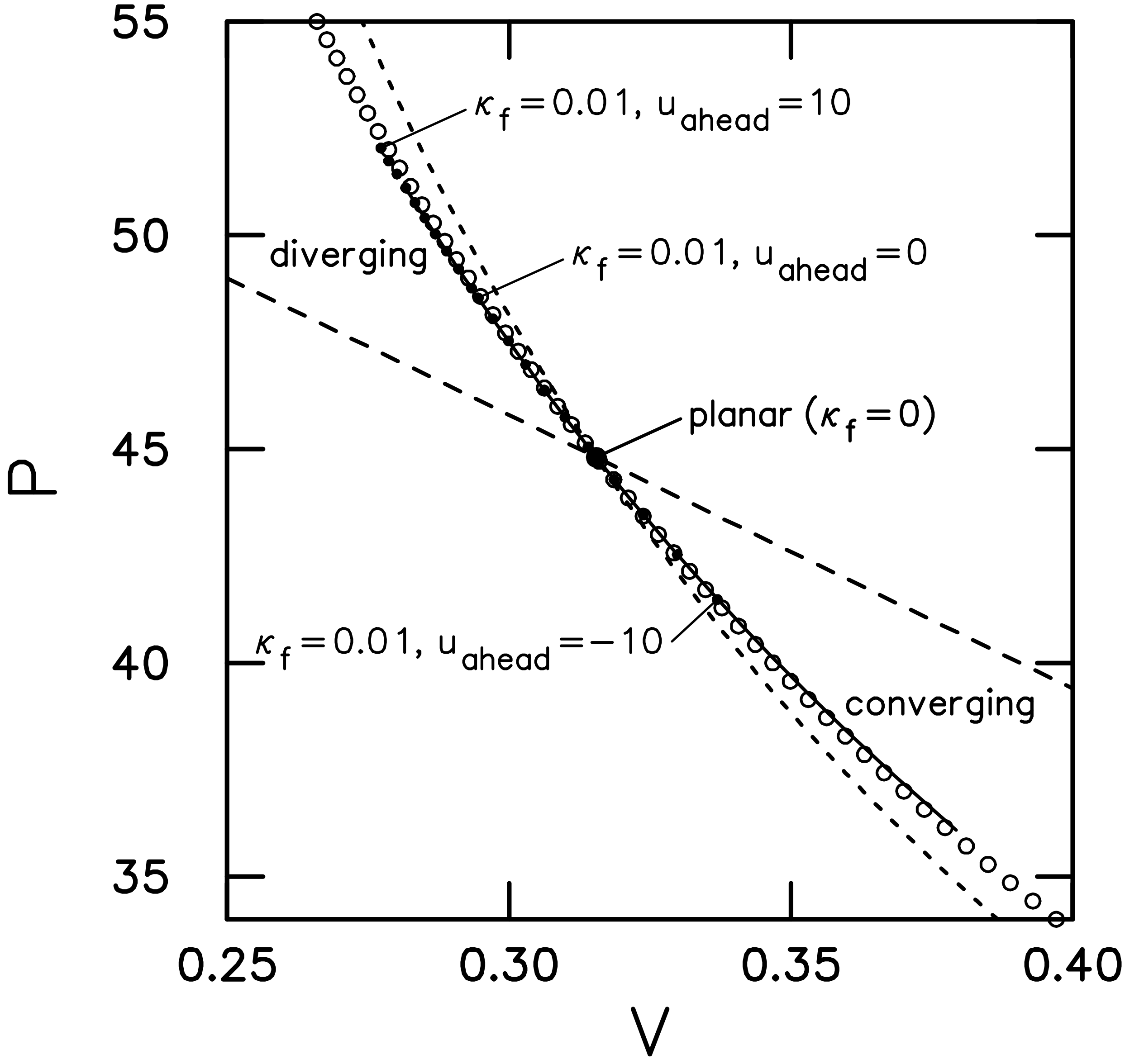

Fig. 8: The loci in P–V plane of states at the end of the reaction zone for a fixed wave speed, $D - u_{\mathrm{ahead}} = 8.0$. The solid line is the locus for $-0.02 \le \kappa_f \le 0.02$ and $u_{\mathrm{ahead}} = 0$. Dots are points on the locus for $\kappa_f = 0.01$ with $-10 \le u_{\mathrm{ahead}} \le 10$. Positive u_{ahead} corresponds to ahead flow away from the shock front. The solid circle is the planar case; $D/D_{\mathrm{CJ}} = 1.17$. The Rayleigh line through the planar state and the planar detonation Hugoniot are shown as a long-dashed and short-dashed line, respectively. The open circles are points on the isentrope through the planar detonation state.

have a corresponding detonation state will change. Hence both parameters are needed to characterize the curvature effect in the detonation wave curve.

To summarize, this example illustrates the following important general properties of curved detonation waves:

1. Front curvature affects all detonation waves; underdriven and overdriven, converging and diverging. The curvature effect is largest for those waves near the minimum detonation speed. A curved detonation wave does not satisfy the standard Hugoniot jump conditions.
2. For a curved detonation wave, the slope of the Rayleigh line in the P–V plane is not proportional to the square of the detonation wave speed.
3. Though the shift in the detonation locus in the P–V plane is small, the shift in the minimum wave speed is significant. For diverging waves, the diameter effect is a consequence of the variation of the minimum detonation wave speed with front curvature.
4. The state behind an underdriven diverging detonation wave corresponds to neither a weak detonation nor to the CJ state on a partially burnt detonation shock Hugoniot. Rather it is determined by the reaction zone dynamics and depends on two parameters κ_f and $\nabla_T \cdot \vec{u}$.

5. Modified Hugoniot Jump Conditions

In the previous section, we described the detonation wave curve for a simple example. Here we show that the qualitative properties for the example hold in general. The key ingredients for the analysis are the modified Hugoniot jump conditions which express the conservation of mass, momentum and energy for a curved detonation wave with non-zero reaction zone width. The correction terms in the Hugoniot jump conditions suggest a natural framework identifying the important parameters that characterize, theoretically and experimentally, the propagation of a curved detonation wave. In addition, we arrive at a natural explanation of numerical errors in simulations with an underresolved reaction zone.

Integrating Eqs. 3.12–3.14 across the reaction zone yields the modified jump conditions

$$\Delta[\rho(D-u)] = \kappa_f w \left\langle \rho u \right\rangle \ , \tag{5.1}$$

$$\Delta\left[\big(\rho(D-u)\big)^2 V + P\right] = \kappa_f w \left\langle \rho(D-u)u \right\rangle \ , \tag{5.2}$$

$$\Delta\left[E + PV + \tfrac{1}{2}(D-u)^2\right] = 0 \ , \tag{5.3}$$

where $\Delta[f] = f(x_0) - f(x_1)$ is the change of variable f across the detonation wave, $w = x_0 - x_1$ is the reaction zone width, and

$$\langle f \rangle = \frac{1}{w}\int_{x_1}^{x_0} dx\, f \tag{5.4}$$

is the average value of f in the reaction zone.

Previously, modified jump conditions were derived directly from the PDEs, Eqs. 3.1–3.3 [13, 14]. The two forms are the same to the accuracy of the quasi-steady approximation $O\big((\kappa_f w)^2\big)$. The above form of the jump conditions are much simpler and they involve fewer averages of the dynamical variables.

The left hand side of Eqs. 5.1–5.3 are the standard planar jump conditions. Since the standard jump conditions hold across the lead shock, the jumps are the same when evaluated for $x = 0^{\pm}$ in front or in back of the lead shock. In this section, we use the subscript 0 to denote the state in front of the lead shock. The right hand side represents a correction to the standard jump conditions due to the non-zero reaction zone width. Because of the quasi-steady approximation, the modified jump conditions are only valid to $O\big((\kappa_f w)^2\big)$. Since the correction terms are all proportional to $\kappa_f w$, the modified jump conditions reduce to the standard jump conditions for either a planar front $\kappa_f = 0$ or a zero reaction zone width $w = 0$.

While $\langle f \rangle \approx \frac{1}{2}[f(0) + f(1)]$ gives a rough estimate of the size of the effect, it is not accurate to $O(\kappa_f w)$ as we assumed in Ref. [13]. Thus, the two integral averages are necessary for the modified jump conditions, and can not be replaced by simple averages of end state values. In general the reaction zone width and the averages depend on the reaction zone dynamics (Figs. 8 and 9) and are slowly varying functions of three parameters; D, κ_f and $\nabla_T \cdot \vec{u}$. Thus in contrast to the standard planar jump conditions, additional information about the reaction zone dynamics is needed for the modified jump conditions.

Since the variation in the mass flux $m = \rho(D - u)$ is $O(\kappa_f w)$, to leading order the mass and momentum jump conditions can be written

$$\Delta[m] = \kappa_f w \, \langle \rho u \rangle \ , \tag{5.5}$$

$$\Delta\left[m^2 V + P\right] = \kappa_f w m_0 \, \langle u \rangle \ , \tag{5.6}$$

where m_0 is the mass flux through the detonation front. The energy jump condition Eq. 5.3 is the Bernoulli equation and is independent of the curvature.

The right hand sides of the jump conditions are not Galilean invariant. They must be evaluated in the distinguished frame for which the quasi-steady ODEs were derived. By Eq. 3.11

$$D = D_0 + \nabla_T \cdot \vec{u}/\kappa_f \tag{5.7}$$

where D_0 is the detonation speed relative to the fluid ahead of the front; *i.e.*, $m_0 = \rho_0 D_0$ is the mass flux through the detonation front. The averages entering the jump conditions can be expressed as

$$\langle \rho u \rangle = \langle \rho \rangle D - m_0 \ , \tag{5.8}$$

$$\langle u \rangle = D - \langle D - u \rangle \ . \tag{5.9}$$

Thus, the jump conditions can be written with the frame dependence in only the wave speed D.

A relation analogous to the Hugoniot function can be derived for a curved detonation wave. We use the algebraic identity

$$\Delta[AB] = \overline{A}\,\Delta[B] + \overline{B}\,\Delta[A]\ , \tag{5.10}$$

where $\overline{A} = \frac{1}{2}\,(A_0 + A_1)$ is the arithmetic average across the reaction zone. Applying this identity to Eq. 5.6 we obtain

$$\overline{(m^2)}\,\Delta V + \overline{V}\,\Delta[m^2] + \Delta P = \kappa_f w\, m_0\,\langle u\rangle\ . \tag{5.11}$$

To leading order

$$\overline{(m^2)} = m_0^2 - m_0\,\Delta[m] \tag{5.12a}$$

$$\Delta[m^2] = 2\,m_0\,\Delta[m] \tag{5.12b}$$

Substituting these relations into Eq. 5.11 we find

$$-\frac{\Delta P}{\Delta V} = m_0^2 + \kappa_f w\,\left(\frac{V_1}{\Delta V}\right)(2\,\langle\rho u\rangle - \rho_1\langle u\rangle)\,m_0\ . \tag{5.13}$$

This is the generalized equation for the "Rayleigh line" which was displayed for our example in Fig. 8.

We note that for a right facing wave $w > 0$ and $m > 0$. Moreover, in the reaction zone both u and ρ are decreasing monotonically behind the front. Therefore, when the ambient fluid is at rest, $u > 0$ and $\langle\rho u\rangle > \rho_1\,\langle u\rangle$. In addition, a detonation wave is compressive $V_0 > V_1$. Consequently, $-\Delta P/\Delta V$ increases with κ_f as shown in Fig. 8.

Applying the identity Eq. 5.10 to the Bernoulli equation we find

$$\Delta E + \Delta[PV] + \tfrac{1}{2}\,\Delta[m^2V^2] = 0$$

$$\Delta E + \overline{P}\,\Delta V + \overline{V}\,\Delta P + \overline{(m^2)}\cdot\overline{V}\,\Delta V + \tfrac{1}{2}\,\overline{(V^2)}\,\Delta[m^2] = 0 \tag{5.14}$$

Then substituting in Eqs. 5.11 and 5.12 we obtain

$$\begin{aligned} \Delta E + \overline{P}\,\Delta V &= \overline{V}\,\left(\overline{V}\,\Delta[m^2] - \kappa_f w\, m_0 \langle u\rangle\right) - \tfrac{1}{2}\,\overline{(V^2)}\,\Delta[m^2] \\ \Delta E + \overline{P}\,\Delta V &= \kappa_f w\, V_0 V_1\, m_0\, \left[\langle \rho u\rangle - \tfrac{1}{2}\,(\rho_0 + \rho_1)\cdot\langle u\rangle\right] \end{aligned} \qquad (5.15)$$

The left hand side of this equation is the standard Hugoniot function.

The correction term on the right hand side of Eq. 5.15 depends on both parameters $\kappa_f w$ and D. As a consequence, a curved detonation wave does not lie on the weak branch of the planar detonation Hugoniot. Because the right hand side of Eq. 5.15 is positive for a diverging wave with the initial state at rest, the wave curve of a diverging detonation wave lies, in the P–V plane, below that of a planar wave. The signs of the correction terms in equations Eqs. 5.13 and 5.15 imply that the curved detonation locus lies between the planar Rayleigh line and the planar detonation Hugoniot as shown in Fig. 8.

The reaction zone width w and the two averages $\langle \rho u\rangle$ and $\langle u\rangle$ are slowly varying functions of the parameters κ_f and $\nabla_T \cdot \vec{u}$. They also vary slowly with the wave strength D_0 (or m_0). Therefore, when the planar Rayleigh line and Hugoniot intersect at non-zero angle, the leading order effect for the end state of a curved detonation can be obtained by linearizing the modified Hugoniot function Eq. 5.15 and the modified Rayleigh line Eq. 5.13.

Let the subscript 1 denote variables at the end state for the planar detonation wave, and denote the correction for κ_f and u_{ahead} by $P = P_1 + \delta P$, etc. The equation of state can be linearized about the planar state (see *e.g.*, Ref. 40 appendix A)

$$\Gamma \delta E = (\gamma - \Gamma)\, P_1 \delta V + V_1 \delta P \qquad (5.16)$$

where $\Gamma = V\,(\partial P/\partial E)_V$ is the Grüneisen coefficient and $\gamma = -\,(\partial \log P/\partial \log V)_S$ is the adiabatic exponent. (For an ideal gas, $\Gamma = \gamma - 1$.) Linearizing Eqs. 5.13 and 5.15, and substituting Eq. 5.16 for δE leads to the equation

$$\begin{pmatrix} \dfrac{\Delta V}{V_1} & -\dfrac{\Delta P}{P_1} \\[2ex] \dfrac{\Delta V}{2V_1} - \dfrac{1}{\Gamma} & -\dfrac{\gamma}{\Gamma} - \dfrac{\Delta P}{2P_1} \end{pmatrix} \begin{pmatrix} \dfrac{\delta P}{P_1} \\[2ex] \dfrac{\delta V}{V_1} \end{pmatrix} = \frac{\kappa_f w\, m_0}{P_1} \begin{pmatrix} \Delta V\,[2\,\langle \rho u\rangle - \rho_1 \langle u\rangle] \\[2ex] V_0\,[\langle \rho u\rangle - \tfrac{1}{2}\,(\rho_0 + \rho_1)\langle u\rangle] \end{pmatrix} \qquad (5.17)$$

The solution to this equation is

$$\begin{pmatrix} \dfrac{\delta P}{P_1} \\[2ex] \dfrac{\delta V}{V_1} \end{pmatrix} = \kappa_f w \, \frac{m_0^2}{\gamma\, P_1/V_1 - m_0^2} \begin{pmatrix} \gamma & \gamma - \dfrac{V_1 \Delta P}{P_1 \Delta V}\,\Gamma \\[2ex] -1 & -(1+\Gamma) \end{pmatrix} \begin{pmatrix} \dfrac{\langle \rho u \rangle}{m_0} \\[2ex] \dfrac{\langle \rho u \rangle - \rho_1 \langle u \rangle}{m_0} \end{pmatrix} \tag{5.18}$$

The denominator $\gamma P_1/V_1 - m_0^2 = \rho_1^2\,[c^2 - (D-u)^2]$ vanishes at the CJ state because it is sonic relative to the front. In this case, Eq. 5.15 needs to be expanded to second order in δP and δV. The solution to the jump conditions at $D = D_{\rm CJ}$ is then given to leading order by

$$\frac{\delta P}{m_0^2} = -\delta V = (\kappa_f w\, V_0 V_1)^{\frac{1}{2}} \left(\frac{m_0 [2\,\langle \rho u \rangle - (\rho_0 + \rho_1) \langle u \rangle]}{m_0^2 - (\partial_V - m_0^2 \partial_P)^2 E} \right)^{\frac{1}{2}} . \tag{5.19}$$

The solution exists only if the square root is real and hence $\kappa_f > 0$. For the ideal equation of state used in our example, $m_0^2 - (\partial_V - m_0^2 \partial_p)^2 E = [(\gamma+1)/(\gamma-1)] m_0^2$.

Geometrically, the linear dependence of δP and δV on $\kappa_f w$ breaks down at $D = D_{\rm CJ}$ because the Rayleigh line and the planar Hugoniot are tangent in the P–V plane. For $\kappa_f > 0$, the curvature of the planar Hugoniot is important since a small shift in the curves leads to a large shift in their intersection point. On the other hand when $\kappa_f < 0$, the correction terms to Eqs. 5.13 and 5.15 shift the Rayleigh line down and the Hugoniot up and there is no intersection point. Thus, Fig. 6 which shows the minimum detonation speed decreasing with curvature is qualitatively true independent of the equation of state and the reaction rate.

Finally, we note that the ratio of the components of the vector on the right hand side of Eq. 5.18 is only independent of $u_{\rm ahead}$ if the averages satisfy the relation $\langle \rho \rangle \cdot \langle D - u \rangle = m_0$. Generally, this relation is only approximately satisfied. Hence, the loci in Fig. 8 when κ_f and $u_{\rm ahead}$ are varied can not be exactly coincident. It is an interesting question as to why the loci are so close, and whether this is specific to the example or a general property of the ODEs for the quasi-steady reaction zone profile.

The modified jump conditions, as shown above, can be used to determine the end state of a curved detonation wave to the accuracy of the quasi-steady approximation $O\big((\kappa_f w)^2\big)$.

Thus, three integral quantities (w, $\langle\rho\rangle$ and $\langle D - u\rangle$ as functions of wave strength) are sufficient to characterize the reaction zone dynamics for propagating a detonation wave. Thus, they provide a more natural description of a real explosive than an effective rate law because they do not introduce any unnecessary details of the micro-physics. In particular, our analysis shows that rate laws can not be uniquely determined only from data on propagating detonation waves. The determination of an effective rate law would require more stringent constraints such as information on the initiation of the explosive.

6. Curvature Effect and Numerical Algorithms

The modified jump conditions developed in the previous section lead to an explanation of the numerical curvature effect illustrated in section 2. Since averages are integral quantities, they are slowly varying functions of front curvature and detonation speed. Moreover, the magnitude of the curvature effect can be estimated by replacing the averages by the arithmetic mean of the front and back of the reaction zone. Thus, the dominant numerical factor that enters into the modified jump conditions is the reaction zone width. Since the correction terms for the jump conditions are proportional to the reaction zone width, the curvature effect increases with this width. For an underresolved reaction zone, the numerical width is larger than the physical width and gives rise to an artificially large numerical curvature effect. Furthermore, when the reaction zone width is proportional to the cell size, the numerical curvature effect is mesh dependent. These numerical effects are displayed in Fig. 1. Similarly, the reaction zone width varies with the orientation of the front and thus, the numerical curvature effect also depends on the orientation. Since these conclusions follow from the conservation laws of the underlying PDEs, a qualitatively similar numerical curvature effect will occur for all explicit numerical algorithms that use a rate equation for the burn model of an explosive. It could, however, be masked by additional errors in a particular difference scheme.

The implication of the curvature effect is that in order to avoid mesh dependent numerical results the reaction zone must be resolved. The example in section 2 shows that a cell size on the order of 0.1 mm is needed to resolve the reaction zone. For applications, the length scale of the bulk flow is typically on the order of 10 cm. The ratio of these length scales is large, 10 cm/0.1 mm = 10^3. A fixed grid is computationally too inefficient and hence impractical. Thus an adaptive grid is required to avoid mesh dependence of the calculated solution. Because of the short time scale in the reaction zone, either a multiple time step algorithm or an implicit scheme is required for efficiency.

An adaptive grid would place a fine mesh around the detonation front and thus in effect would be a form of tracking. Unlike true front tracking, adaptive mesh refinement does not make use of the inherent simplifications discussed in the previous sections which apply when $\kappa_f w$ is small. Moreover, due to the short length and time scales, calculating the fine details of the reaction zone structure greatly increase the computational effort. The fine details, as discussed in the next section, are typically beyond the accuracy of the reaction model and thus are of questionable value for a real explosive. Therefore, an adaptive grid is an inefficient method for eliminating the mesh dependence of propagating detonation waves.

6.1 Transverse instabilities

For the reactive flow equations, the reaction zone of a detonation wave is subject to a 2-D transverse instability. The instability has been observed experimentally (see e.g., Ref. 1, chpt. 7) in gaseous explosives. For heterogeneous explosives a related phenomenon is the propagation of perturbations from multi-point initiation over large distances relative to the reaction zone width with little smoothing. A linear analysis of the reactive Euler equations shows the instability [41–43]. The instabilities also occur in numerical calculations when the reaction zone is highly resolved [16–18].

Both the experiments and the simulations show that the amplitude of the instability saturates. On a scale large compared to both the width of the reaction zone and the wavelength of the instability, the detonation front is well defined. With sufficient numerical smoothing the reaction zone instability can be eliminated. Several forms of numerical smoothing commonly occur in finite difference algorithms: (i) With an underresolved reaction zone the grid provides a spatial cutoff at wavelengths $\lambda < 2\Delta x$ and a temporal cutoff at frequencies $\nu > c/\Delta x$. (ii) In Eulerian schemes or with adaptive meshes, advection is diffusive and has an effect similar to viscosity or heat conduction. (iii) To minimize truncation errors at discontinuities (shocks) some form of numerical dissipation is added; *e.g.*, artificial viscosity or Riemann solvers. However, numerical smoothing can have side effects on propagating a detonation wave. In order to match the experimental propagation data for a real explosive, artificial numerical smoothing would require the rate model to be calibrated to the particular algorithm. This is an extension of the fact that the numerical model equation of state can affect the calibration of a rate law.

6.2 Empirical Reaction Rates

There is an additional reason for using an empirical burn model. The reaction chemistry can be very complicated involving many short lived intermediate species with a large number of reactions. The reaction kinetics is not well enough understood to determine the rates from first principles. Moreover, the reactions occur on a short time scale which is difficult to measure experimentally. In addition, many explosives of interest are heterogeneous materials, such as plastic bonded explosives. They have length scales associated with the crystal size and pore size. The sensitivity of rates to temperature suggests that hot spots from imploding pores may dominate the reaction zone dynamics.

Transverse waves in the reaction zone of a real explosive give rise to a complex structure with short wavelength fluctuation. The energy density or pressure is too high to enable fingering type instabilities to grow very large. Thus, the amplitude of the instability must saturate. The fact that the experimentally measured detonation front is usually well behaved over long wavelengths indicates that the short wavelength fluctuations in the reaction zone must average out [16]. Exceptional cases when the fluctuations are important, such as near the failure diameter in a rate stick [44], are beyond the scope of this paper. When the fluctuations do average out, their effect on a propagating detonation wave is factored into the calibration of an empirical rate law. This is quite reasonable in view of the modified jump conditions which imply the detonation Hugoniot only depends on a few average quantities in the reaction zone. Using an effective rate law to account for short wavelength reaction zone fluctuations is analogous to using a Reynolds stress to account for turbulent eddies in a non-reactive flow.

Assuming a single reaction progress variable for the burn model is a gross oversimplification. The most one can hope for is empirically to fit data on propagating waves. Because of the sensitivity of the transverse instabilities to the model reaction rate, the fine details of the the reaction zone in highly resolved calculations can not possibly be physically accurate and quantitatively describe a real explosive. At best they can give the statistics of the short wavelength fluctuations. Thus, for applications, a highly resolved reaction zone is computationally wasteful and often impractical. Furthermore, the transverse structure in a highly resolved calculation may effect the calibration of an empirical rate law and cause it to be mesh dependent.

7. Tracking Algorithms

For reliable numerical simulations it is mandatory that calculated results be independent of the computational mesh. When initiation is not an issue, there is an alternative to capturing algorithms which use empirical rate laws, track a detonation wave with an adaptive grid, and rely on artificial numerical smoothing for stability. There are two algorithms that explicitly track a detonation wave: Detonation Shock Dynamics[10–12] and Front Tracking [21]. Rather than resolving the reaction zone these algorithms directly incorporate the empirical data on wave propagation. In effect, they cleanly separate the hydrodynamic length scales from the subgrid length scale which can not be modeled in detail.

7.1 Detonation Shock Dynamics

Detonation shock dynamics is appropriate for propagating underdriven diverging detonation waves. The algorithm is based on the special property that the flow behind an underdriven detonation wave is supersonic relative to the front. Hence acoustic waves from behind can not catch up to and affect the dynamics of an underdriven detonation wave. An additional assumption in the DSD algorithm is that the state in front of the wave is constant. In typical applications with a solid explosive, the ambient flow ahead of the detonation is at rest and the additional assumption is satisfied. In this case, since the detonation is self-sustaining, the front decouples from the rest of the flow.

The motion of the front is determined by the local detonation speed which is a function only of the front curvature, $D(\kappa_f)$ [10, 11]. If $D(\kappa_f) = D_{\text{CJ}}$ for all κ_f, then DSD reduces to the programmed burn model. Thus DSD is a generalization of programmed burn which accounts for the curvature effect of an underdriven detonation wave.

The key function $D(\kappa_f)$ can be determined either experimentally, *e.g.*, from rate stick experiments, or be computed from a rate law by solving the eigenvalue problem for the quasi-steady reaction zone profile [9]. To calculate the fluid flow resulting from the detonation wave, the state behind the detonation wave is needed. This state is not arbitrary and for a curved detonation wave it is not the planar CJ state. The state behind the detonation wave must be consistent with the modified Hugoniot jump conditions. Otherwise, the burn front and the lead hydrodynamic shock of the detonation wave separate and the algorithm becomes unstable unless *ad hoc* numerical correction terms are added. Details of implementing the DSD algorithm and in particular the energy release behind the sonic point and the effect of boundaries can be found in Refs. 12, 45, 46.

The flow behind an overdriven detonation wave is subsonic and the decoupling of the detonation front, which is the key assumption in DSD, is no longer valid. An extreme example is a converging detonation wave in cylindrical or spherical geometry. To leading order the detonation speed is a function of the ratio of the initial radius at which the detonation wave was initiated to the current radius of the detonation front, see *e.g.*, Ref. 22, pp. 121–125. With DSD, the detonation speed could only be a function of the radius. DSD is not applicable in this example because the coupling with the converging flow behind the detonation is important. Even in steady-state, overdriven detonation waves can occur and have been observed; see, [26], chpt. XI, sec. 2.2.

7.2 Front Tracking Method

Front tracking accounts for the coupling between the motion of the front and the flow behind it. The front is propagated by solving a non-local Riemann problem [19, 20, 47]. This is a significant advance over Whitham's shock propagation scheme because there is no approximation on the incoming characteristic. The analytic information which characterizes the wave dynamics is contained in the wave curve. Thus, the curvature effect is incorporated by using the curved detonation wave curve instead of the planar detonation shock Hugoniot.

The coupling of the detonation front with the hydrodynamics has a stabilizing effect on the wave propagation. If during one time cycle the front speed is too large then the wave becomes underdriven and slows down. On the other hand if the wave speed is too slow then the wave becomes overdriven and speeds up. The front tracking algorithm is simplified by tracking only the lead detonation wave and capturing the weaker waves that follow. The energy release and adiabat set by the dominant detonation wave is important for an accurate numerical simulation.

The curvature effect introduces a new aspect to the front tracking algorithm. Compared to a shock, the detonation wave curve depends on two additional parameters; the local front curvature and the flow divergence ahead of the wave. For numerical stability, the front must be smooth with a slowly varying curvature. Without additional dynamical degrees of freedom on the front (corresponding to the mass, momentum and energy in the reaction zone) the algorithm will have an error in total conservation on the order of the accuracy of the quasi-steady approximation $O\big((\kappa_f w)^2\big)$. Typically a detonation wave will fail to propagate when $\kappa_f w$ is a few percent. Thus, the error in conservation is expected to be $<< 0.1\%$. Usually, equations of state and the chemical energy released by an explosive are not known to this accuracy. Since a material can only burn once, the energy error does not accumulate. We believe the slight error in conservation is less important than propagating the detonation wave with the correct speed.

Another important aspect of front tracking is wave interactions [48, 49]. Interactions involving a detonation wave can have anomalous properties due to the reaction zone width. At the interface with a low impedance media (*e.g.*, an unconfined rate stick), in the frame of the node the detonation wave becomes sonic and the wave pattern is similar to an anomalous reflection [50, 51], see also Ref. 5, appendix C and Ref. 45, p. 781.

Another example is the experimental observation that the interaction of two oblique detonation waves does not give the expected Mach wave pattern [32]. We note that the shock polar analysis applied separately to the lead shock and the detonation wave gives different results for the wave angles. A likely explanation of the inconsistency is that the shock polar analysis does not apply to a detonation wave because of its non-zero width. Instead of a point-like wave interaction on which the shock polar analysis is based, the wave front curves and the interaction is spread out in a manner similar to what occurs in von-Neumann reflection [52]. In the region of high curvature, the tangential flow within the reaction zone is not small and the 1-D assumption on which the wave curve is based breaks down. Even though a robust finite difference algorithm gives an answer which may even appear to converge under mesh refinement, the numerical results are not necessarily correct. Front tracking encourages the analysis necessary to understand these problems.

8. Conclusion

We have developed modified Hugoniot jump conditions for propagating detonation waves which account for both front curvature and reaction zone width. Of the entire reaction zone dynamics only three integral quantities determine the propagation of a detonation wave. These are the reaction zone width and the averages of ρ and ρu. The modified jump conditions are a direct consequence of the conservation laws and thus apply irrespective of the details of reaction dynamics.

For a model to describe correctly the propagation of detonation waves it must lead to accurate values for the three integral quantities. This is difficult to achieve with numerical finite difference schemes. Unless the reaction is well resolved, the integral quantities (in particular w) are strongly mesh dependent, leading to an artificially large curvature effect. On the other hand, for a well resolved reaction zone the relationship between the underlying rate law and the integral quantities is complicated by high frequency transverse instabilities. The uncertainties in the microstructure and incomplete knowledge about the chemical reactions make the detailed structure of a resolved reaction zone of questionable value. Furthermore, the parameters in the rate law likely depend on the degree to which these instabilities are resolved. This leads to the unsavory choice of either a mesh dependent wave propagation or a mesh dependent reaction rate. Another facet of this dilemma is that one either calculates with manifestly incorrect integral quantities or incorporates physically questionable and computationally costly detail into the simulation.

Front tracking is a solution to this problem. Instead of capturing or trying to resolve the reaction zone, the detonation wave can be tracked. The propagation of a detonation wave is characterized by a wave curve which depends on front curvature and the velocity divergence ahead of the detonation wave. This approach requires an empirical determination of the integral quantities which enter into the jump conditions. Tracking gives a clean separation of the different length scales and can reproduce empirical data on wave propagation without relying on a detailed model for the microstructure which is currently unknown.

This work was supported by the U. S. Department of Energy.

REFERENCES

1. Fickett, W. and Davis, W. C., *Detonation*, Univ. of California Press, Berkeley, 1979.
2. Eyring, H., Powell, R. E., Duffey, G. H. and Parlin, R. B., *The Stability of Detonation*, Chem. Rev. 45:69–181 (1949).
3. Wood, W. W. and Kirkwood, J. G., *Diameter Effect in Condensed Explosives: The Relation between Velocity and Radius of Curvature of the Detonation Wave*, J. Chem. Phys. 22:1920–1924 (1954).
4. Campbell, A. W. and Engelke, R., *The Diameter Effect in High-Density Heterogeneous Explosives*, Proceedings Sixth International Symposium on Detonation, Office of Naval Research, Coronado, CA., 1976, pp. 642–652.
5. Bdzil, J. B., *Steady-State Two-Dimensional Detonation*, J. Fluid Mech. 108:195–226 (1981).
6. Stewart, D. S. and Bdzil, J. B., *The Shock Dynamics of Stable Multidimensional Detonation*, Combust. Flame 72:311–323 (1988).
7. Jones, J., *The Spherical Detonation*, Adv. Appl. Math. 12:147–186 (1991).
8. Bukiet, B. and Jones, J., *The Competition Between Curvature and Chemistry in a Spherically Expanding Detonation*, Appl. Phys. Letters 52:1921–1923 (1988).
9. Bukiet, B., *The Effect of Curvature on Detonation Speed*, SIAM J. Appl. Math. 49:1433–1446 (1989).
10. Bdzil, J. and Stewart, D. S., *Modeling Two-Dimensional Detonations with Detonation Shock Dynamics*, Phys. Fluids A 1:1261–1267 (1989).
11. Bdzil, J., Fickett, W. and Stewart, D. S., *Detonation Shock Dynamics: A New Approach to Modeling Multi-Dimensional Detonation Waves*, Proceedings of the Ninth International Symposium on Detonation, Office of Naval Research, Portland, OR, 1989, pp. 730–742.
12. Lambourn, B. D. and Swift, D. C., *Application of Whitham's Shock Dynamics Theory to the Propagation of Divergent Detonation Waves*, Proceedings of the Ninth International Symposium on Detonation, Office of Naval Research, Portland, OR, 1989, pp. 784–797.
13. Bukiet, B. G. and Menikoff, R., *Detonation Waves and the Front Tracking Method*, Phys. Fluids A 4:2070–2081 (1992).
14. Bukiet, B. G., Lackner, K. S. and Menikoff, R., *Understanding Curved Detonation Waves*, Proceedings of the Tenth International Symposium on Detonation, Office of Naval Research, Boston, MA, 1993.

15. Donguy, P. and Legrand, N., *Numerical Simulations of Non-Ideal Detonations of a Heterogeneous Explosive with the Two Dimensional Eulerian Code C.E.E.*, Proceedings of the Seventh International Symposium on Detonation, Office of Naval Research, Annapolis, MD, 1981, pp. 695–702.

16. Schöffel, S. U. and Ebert, F., *Numerical Analyses Concerning the Spatial Dynamics of an Initially Plane Gaseous ZND Detonation*, in International Colloquium on Dynamics of Explosions and Reactive Systems (A. L. Kuhl, Ed.), Progress in Astronautics and Aeronautics, 114, AIAA, Washington, 1988, pp. 3–31.

17. Oran, E. S., Kailasanath, K. and Guirguis, R. H., *Numerical Simulations of the Development and Structure of Detonations*, in International Colloquium on Dynamics of Explosions and Reactive Systems (A. L. Kuhl, Ed.), Progress in Astronautics and Aeronautics, 114, AIAA, Washington, 1988, pp. 155–169.

18. Bourlioux, A. and Majda, A. J., *Theoretical and Numerical Structure for Unstable Two-Dimensional Detonations*, Combust. Flame 90:211–229 (1992).

19. Glimm, J., Isaacson, E., Marchesin, D. and McBryan, O., *Front Tracking for Hyperbolic Systems*, Adv. Appl. Math. 2:91–119 (1981).

20. Chern, I.–L., Glimm, J., McBryan, O., Plohr, B. and Yaniv, S., *Front Tracking for Gas Dynamics*, J. Comp. Phys. 62:83–110 (1986).

21. Bukiet, B., *Application of Front Tracking to Two Dimensional Curved Detonation Fronts*, SIAM J. Sci. Stat. Comp. 9:80–99 (1988).

22. Mader, C., *Numerical Modeling of Detonations*, Univ. of California Press, Berkeley, 1979.

23. Mader, C. L. and Forest, C. A., *Two-Dimensional Homogeneous and Heterogeneous Detonation Wave Propagation*, Los Alamos Scientific Laboratory report, LA-6259, 1976.

24. Ramsay, J. B. and Popolato, A., *Analysis of Shock Wave and Iniation Data for Solid Explosives*, Proceedings of the Fourth International Symposium on Detonation, Office of Naval Research, White Oak, MD, 1965, pp. 233–238.

25. Klein, R., *On the Dynamics of Weakly Curved Detonations*, in Dynamical Issues in Combustion Theory (P. C. Fife, A. Liñán and F. A. Williams, Eds.), IMA volumes in Mathematics and its Applications, Vol. 35, Springer-Verlag, N.Y., 1991, pp. 127–166.

26. Chéret, R., *Detonation of Condensed Explosive*, Springer-Verlag, New York, 1993.

27. Erpenbeck, J. J., *Steady-State Analysis of Quasi-One-Dimensional Reactive Flow*, Phys. Fluids 11:1352–1370 (1968).

28. Erpenbeck, J. J., *Steady Quasi-One-Dimensional Detonations in Idealized Systems*, Phys. Fluids 12:967–982 (1969).

29. Fujiwara, T. and Tsuge, S., *Quasi-One-Dimensional Analysis of Gaseous Free Detonations*, J. Phys. Soc. Japan 33:237–241 (1972).

30. DeVore, C. R. and Oran, E. S., *The Stability of Imploding Detonations in the Geometrical Shock Dynamics (CCW) Model*, Phys. Fluids A 4:835–844 (1992).

31. Oran, E. S. and DeVore, C. R., *The Stability of Imploding Detonations: Results of Numerical Simulations*, Phys. Fluids 6:369–380 (1994).

32. Lambourn, B. D. and Wright, P. W., *Mach Interaction of Two Plane Detonation Waves*, Proceedings of the Fourth International Symposium on Detonation, Office of Naval Research, White Oak, MD, 1965, pp. 142–152.

33. Souletis, J. and Groux, J., *Continuous Observation of Mach Bridge and Mach Phenomena*, Proceedings of the Eigth International Symposium on Detonation, Office of Naval Research, Albuquerque, NM, 1985.

34. Wood, W. W. and Salsburg, Z. W., *Analysis of Steady-State Supported One-Dimensional Detonations and Shocks*, Phys. Fluids 3:549–566 (1960).

35. Huerta, M. A., *Steady Detonation Waves with Losses*, Phys. Fluids 28:2735–2743 (1985).

36. Erpenbeck, J. J., *Stability of Idealized One-Reaction Detonations*, Phys. Fluids 7:684–696 (1964).

37. Erpenbeck, J. J., *Stability of Steady-State Equilibrium Detonations*, Phys. Fluids 5:604–614 (1962).

38. Tsuge, S., Fujiwara, T., Matsukawa, M. and Nakagawa, T., *On the Dual Property and the Limit of Hydrogen-Oxygen Free Detonation Waves*, Astronautic Acta. 15:377–386 (1970).

39. Tsuge, S., *The Effect of Boundaries on the Velocity Deficit and the Limit of Gaseous Detonations*, Combustion Science and Technology 3:195–205 (1971).

40. Menikoff, R. and Plohr, B., *Riemann Problem for Fluid Flow of Real Materials*, Revs. Mod. Phys. 61:75–130 (1989).

41. Erpenbeck, J. J., *Detonation Stability for Disturbances of Small Transverse Wavelength*, Phys. Fluids 9:1293–1306 (1966).

42. Erpenbeck, J. J., *Nonlinear Theory of Unstable Two-Dimensional Detonation*, Phys. Fluids 13:2007–2026 (1970).

43. Abouseif, G. E. and Toong, T.–Y., *Theory of Unstable Two-Dimensional Detonations: Genesis of the Transverse Waves*, Combust. Flame 63:191–207 (1986).

44. Dremin, A. N. and Trofimov, V. S., *Nature of the Critical Detonation Diameter of Condensed Explosives*, Fizika Goreniya i Vzryva 5:304–311 (1969). Engl. transl., Combustion, Explosion and Shock Waves 5:208–212 (1969).

45. Bdzil, J. and Stewart, D. S., *Examples of Detonation Shock Dynamics for Detonation Wave Spread Applications*, Proceedings of the Ninth International Symposium on Detonation, Office of Naval Research, Portland, OR, 1989, pp. 773–783.

46. Bdzil, J. and Fickett, W., *DSD Technology: a Detonation Reactive Huygens Code*, Los Alamos National Laboratory report, LA-12235-MS, 1992.

47. Chern, I-L. and Colella, P., *A Conservative Front Tracking Method for Hyperbolic Conservation Laws*, Lawrence Livermore National Laboratory, Preprint UCRL-97200, 1987.

48. Glimm, J., Klingenberg, C., McBryan, O., Plohr, B., Sharp, D. and Yaniv, S., *Front Tracking and Two Dimensional Riemann Problems*, Adv. Appl. Math. 6:259–290 (1985).

49. Grove, J., *The Interaction of Shock Waves with Fluid Interfaces*, Adv. Appl. Math. 10:201–227 (1989).

50. Grove, J. W. and Menikoff, R., *Anomalous Reflection of a Shock Wave at a Material Interface*, J. Fluid Mech. 219:313–336 (1990).

51. Menikoff, R., *Determining Curvature Effect on Detonation Velocity from Rate Stick Experiment*, IMPACT 1:168–179 (1989).

52. Colella, P. and Henderson, L. F., *The von Neumann Paradox for the Diffraction of Weak Shock Waves*, J. Fluid Mech. 213:71–94 (1990).